

Criticality and Quench Dynamics at the Anderson Transition of a Chern Insulator

L. Ulčakar,^{1,2,*} J. Mravlje,^{2,1} G. Lemut,³ and T. Rejec^{1,2}

¹*University of Ljubljana, Faculty of Mathematics and Physics, Jadranska 19, Ljubljana, Slovenia*

²*Jožef Stefan Institute, Jamova 39, Ljubljana, Slovenia*

³*Dahlem Center for Complex Quantum Systems,
Halle-Berlin-Regensburg Cluster of Excellence CCE, and Fachbereich Physik,
Freie Universität Berlin, Arnimallee 14, 14195 Berlin*

(Dated: June 3, 2026)

We study the critical properties of the topological Anderson phase transition in a strongly disordered Chern insulator, separating the topological phase from a trivial Anderson insulator. We show that the transition is characterized by a non-zero electrical conductance and by the emergence of a critical length scale in the real-space profile of the local Chern marker. From this, we extract the correlation-length and the dynamical critical exponents, which are consistent with those of non-interacting models of the integer quantum Hall effect. We then ramp the disorder strength across the transition and study the ensuing dynamics. In contrast to clean topological systems, we find that the excitation density does not follow the Kibble-Zurek scaling. The non-equilibrium length scale associated with the local Chern marker is decoupled from the generation of excitations. For studied system sizes, we find it to be close to the Kibble-Zurek prediction for the topological-to-trivial quench, while it deviates from it for the reverse direction.

I. INTRODUCTION

Chern insulators are renowned for the presence of robust electronic edge states and the quantum anomalous Hall (QAH) effect. These properties are a consequence of a non-trivial band topology, which protects them against dissipation [1–4]. Numerical studies have shown however that strong enough disorder in the bulk can destroy the topological phase due to Anderson localization [5, 6]. The phase transition into a trivial Anderson insulator is of second order and is signaled by the vanishing of the Chern number [7, 8]. Previous numerical studies of disordered Chern models have shown that the transition is consistent with the universality class of the integer quantum Hall effect (IQHE) [9–11], with the localization length diverging with a critical exponent $\nu \approx 2.3–2.6$ [7, 8, 12–14]. These findings were based on scaling analyses of the Chern number and the direct-current conductivity. An open question is whether this length scale is directly reflected in the spatial structure of local observables, such as the local topological marker, or instead remains obscured by disorder. The dynamical critical exponent also remains unexplored in topological system.

Similarly, non-equilibrium dynamics following quenches across transitions between distinct Anderson-localized phases has not been studied yet. Quench dynamics has been extensively studied in topological band insulators [15–29]. These works showed that even slow quenches generally drive the system out of equilibrium due to the closing of the band gap at the critical point. In translation-invariant systems, the dynamics near the gap closing can be described by Landau–Zener band crossing, which is directly connected to the Kibble–Zurek (KZ) mechanism [30, 31]. This non-equilibrium paradigm describes the dynamics as adiabatic except close to the critical point, where it is effectively frozen. Consequently, the non-equilibrium length scale and its associated topological defects inherit the properties of the critical point reflected in the scaling determined by the critical exponents. In translation-invariant topological systems, the excitation density and characteristic length scale obey universal KZ scaling relations [25, 26, 32, 33]. Recent studies further demonstrated that weak disorder induces spatial inhomogeneities in real-space topological markers that are characterized by a length scale consistent with KZ predictions [34–36]. An important open question is whether this non-equilibrium picture remains valid for transitions driven by strong disorder, where the dynamics cannot be captured by the collective Landau–Zener description of band crossings as in translation-invariant systems, but is instead governed by a large number of coupled localized states [37].

In this work we investigate the critical behaviour of the Anderson localization transition and the non-equilibrium dynamics following quenches across it in a disordered Chern insulator. We first

characterize the phase diagram by calculating the electrical conductance and the Chern number. From finite-size scaling we extract the correlation-length and dynamical critical exponents and find them to be consistent with the universality class of the IQHE in non-interacting systems. We further show that a universal length scale emerges in the real-space profile of the local Chern marker (LCM). We then study finite-time quenches of the disorder strength across the transition, starting from the ground state in either the topological phase or the trivial Anderson localized phase. We show that the resulting excitation density exhibits only a weak power-law dependence on the quench time and deviates from the KZ prediction. The non-equilibrium LCM length scale exhibits differing behaviour depending on the direction of the quench. For studied system sizes, the length scale is close to the KZ scaling for the topological-to-trivial direction, while for quenches in the opposite direction the length scale deviates from the KZ predictions.

The paper is structured as follows. In Sec. II we introduce the model and methods. In Sec. III we inspect the topological properties through the LCM, the conductance and the spectral statistics. In Sec. IV, we extract the dynamical and the correlation length critical exponents. In Sec. V, we present the dynamics following a disorder quench by analyzing the profile of the LCM and the density of excitations. In Sec. VI, we discuss the results and conclude the paper.

II. THE MODEL AND METHODS

We study an Anderson localization phase transition in a Chern insulator described by the half-filled disordered Qi-Wu-Zhang (QWZ) model [38]

$$\hat{H} = \sum_{\mathbf{r}} |\mathbf{r}\rangle\langle\mathbf{r}| \otimes (u \hat{\sigma}_z + W(\mathbf{r}) \hat{\sigma}_0) + \sum_{\mathbf{r}, j \in \{x, y\}} \left(|\mathbf{r} + \mathbf{e}_j\rangle\langle\mathbf{r}| \otimes \frac{\hat{\sigma}_z + i \hat{\sigma}_j}{2} + \text{h.c.} \right) \quad (1)$$

where $\mathbf{r} = (x, y)$ are the Bravais lattice vectors of a square lattice, measured in units of the lattice constant, and \mathbf{e}_j are Cartesian unit vectors. The system size is $N \times N$ unit cells and periodic boundary conditions are assumed. Each unit cell hosts two orbitals $|\mathbf{r}\alpha\rangle$, $\alpha \in \{A, B\}$, and the Pauli matrices $\hat{\sigma}_i$, $i \in \{x, y, z\}$, act on these orbital degrees of freedom. $W(\mathbf{r})$ is the electrostatic disorder that is uncorrelated and uniformly distributed on the interval $[-W/2, W/2]$. In the following, the system size is set to $N = 100$ and results are averaged over 100 disorder realizations, unless explicitly specified otherwise.

We characterize the topological phases of inhomogeneous states by calculating the LCM. The LCM is a real-space analogue of the Berry curvature and was shown to reflect critical behaviour of the topological phase transitions in disordered systems [34, 39]. It is defined as [40]

$$c(\mathbf{r}) = 2\pi i \sum_{\alpha} \langle \mathbf{r}\alpha | \hat{P} [-i[\hat{x}, \hat{P}], -i[\hat{y}, \hat{P}]] | \mathbf{r}\alpha \rangle, \quad (2)$$

where $\hat{P} = \sum_n |\Psi_n\rangle\langle\Psi_n|$ is the projector onto the subspace spanned by occupied states $|\Psi_n\rangle$. For a system with periodic boundary conditions, $-i[\hat{x}, \hat{P}]$ is expressed with finite differences as proposed in Ref. [5]. The Chern number is then $C = \lim_{N \rightarrow \infty} \frac{1}{N^2} \sum_{\mathbf{r}} c(\mathbf{r})$ [40].

We additionally characterize the state by examining the two-terminal conductance G of the system [41]. Periodic boundary conditions are assumed in the other direction. The electrical conductance is calculated from the transmission matrix $\hat{t}(E)$ for scattering states at energy E as $G(E) = G_0 \text{tr}(\hat{t}^\dagger(E)\hat{t}(E))$, where $G_0 = e^2/h$ is conductance quantum, h is Planck constant and e is the electron charge.

In order to inspect the dynamical critical properties, we also calculate the linear-response alternating-current (AC) conductivity in the limit of linear response. It characterizes the response of the system to an oscillating electrical field with frequency ω . Its real part is expressed as:

$$\sigma_{xx}(\omega) = - \lim_{\eta \rightarrow 0} \frac{e^2 \hbar}{N^2} \sum_{m \neq n} \frac{f(E_m) - f(E_n)}{E_m - E_n} |\langle \Psi_m | \hat{v}_x | \Psi_n \rangle|^2 \frac{\eta}{(E_m - E_n - \hbar\omega)^2 + \eta^2}. \quad (3)$$

Here, $\hat{v}_x = i/\hbar[\hat{H}, \hat{x}]$ is the velocity operator in x -direction, $f(\varepsilon)$ is the Fermi-Dirac occupation function, and E_n and $|\Psi_n\rangle$ are the eigenenergies and eigenstates, respectively. For numerical simulations of finite systems, η should be of the order of the energy level spacing. We set it to $\eta = 15/N^2$.

III. PHASE DIAGRAM

In the absence of disorder, the system is in a topologically non-trivial insulating phase with $C = \text{sgn}(u)$ for $|u| < 2$ and a trivial insulating phase for $|u| > 2$. As shown in Fig. 1(a) and demonstrated in previous works [5, 7, 8, 13, 14], the topologically non-trivial phase persists until large values of disorder. We set $u = -1$ throughout the paper, in which case the system becomes a trivial insulator at $W_c = 6.01 \pm 0.02$ as estimated from the maximum of electrical conductance.

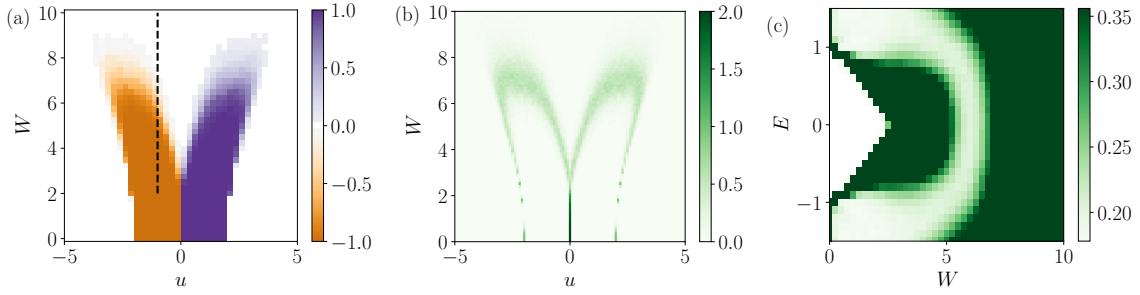


FIG. 1. Phase diagram in the (u, W) parameter space of the (a) Chern number and (b) the electrical conductance. (c) The energy level-spacing variance of the states per energy window of width 0.1, at $u = -1$. Data is averaged over (a) 10, (b) 50 and (c) 100 disorder realizations. Dashed line indicates the values of parameters during the quench.

The electrical conductance at the Fermi level is shown in Fig. 1(b). The system is an insulator except along the boundary separating phases with different Chern numbers. There, the system is conducting with conductance equal to half of conductance quantum $G_0/2$.

The existence of the non-zero conductance and its connection to the phase diagram can be explained by inspecting the localization properties through the energy level statistics. According to the random matrix theory [42], energy levels of localized states are distributed randomly inside an energy window following the Poisson distribution $P_P(s) = e^{-s}$. The level-spacing variance $\langle s^2 \rangle - \langle s \rangle^2$ is of the order of 1. Level statistics of extended states, on the other hand, follows the Wigner-Dyson distribution $P_{\text{WD}}(s) = \frac{32s^2}{\pi^2} e^{-4s^2/\pi^2}$, with level-spacing variance equal to 0.178. In Fig. 1(c), we show level-spacing variance for a system at $u = -1$ and varying W and energy E . For low disorder strengths, the system has a band gap and all states are extended. Increasing disorder strength above $W = 2.5$ creates localized states inside the former band gap, and the extended states (light green) that define the mobility gap travel towards $E = 0$. The extended states reach Fermi level at $W = W_c$, which corresponds to the increase of the Chern number to -0.5 and to $G_0/2$ conductance. For $W > W_c$, there are no more extended states in the system, which marks the topological Anderson phase transition to a trivial Anderson insulator.

IV. CRITICAL SCALING

To characterize the topological Anderson phase transition, we investigate the universal behaviour of conducting and topological properties and from them extract the correlation length ξ and the relaxation time τ_r . Close to the critical point, these are expected to be power-law functions of disorder strength

$$\xi(W) \propto |W - W_c|^{-\nu}, \quad \tau_r(W) \propto \xi(W)^z \propto |W - W_c|^{-\nu z}. \quad (4)$$

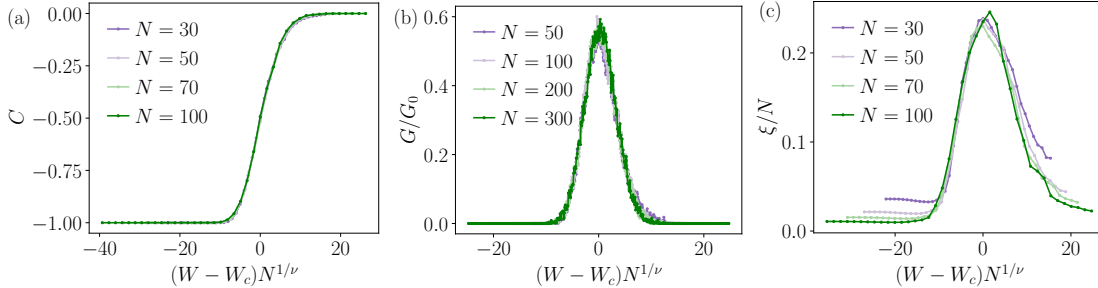


FIG. 2. Finite-size scaling plots across the phase transition of (a) the Chern number, (b) the electrical conductance and (c) the correlation length ξ/N estimated from the LCM profile. Quantities are presented as functions of the rescaled control parameter $(W - W_c)N^{1/\nu}$ for different system sizes.

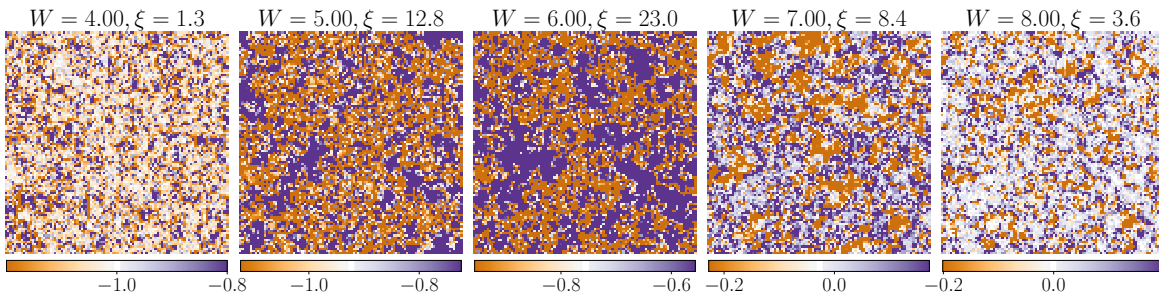


FIG. 3. Real-space profile of the local Chern marker of the ground state at different disorder strengths that range across the phase transition.

The power exponents z and ν are termed the dynamical and the correlation-length critical exponent, respectively. Critical behaviour is important to understand also for systems out of equilibrium. For clean topological systems that are driven with a finite rate across the critical point, it was shown that the critical behaviour is imprinted in system's non-equilibrium properties through the KZ mechanism [25, 26, 32, 33].

A. Correlation length critical exponent

The correlation-length critical exponent ν is inferred from finite-size scaling of quantities, whose critical behaviour is governed by the divergence of the correlation length. In a finite system of linear size N , this divergence is cut off by N , such that observables depend on the ratio N/ξ . For observables that exhibit single-parameter scaling, this leads to the scaling form

$$f(W, N) = F(|W - W_c|N^{1/\nu}), \quad (5)$$

where F is a universal scaling function and f is the considered quantity. We identify this behaviour in both the Chern number and the linear electrical conductance, as shown in Fig. 2(a) and Fig. 2(b). By optimizing the collapse of the rescaled data with respect to the exponent ν , we obtain $\nu = 2.7 \pm 0.1$ from the conductance and $\nu = 2.5 \pm 0.1$ from the Chern number. The optimal value is determined by minimizing the χ^2 cost function across all combinations of system sizes, with the reported estimate given by the mean and the uncertainty by the corresponding standard deviation of the optimal values obtained from each size combination.

In the following, we show that the critical length scale appears also in the real-space profile of the LCM. Its profile becomes highly inhomogeneous as disorder strength is increased, see Fig. 3. System consists of regions, where the LCM deviates above and below the average value. The typical size

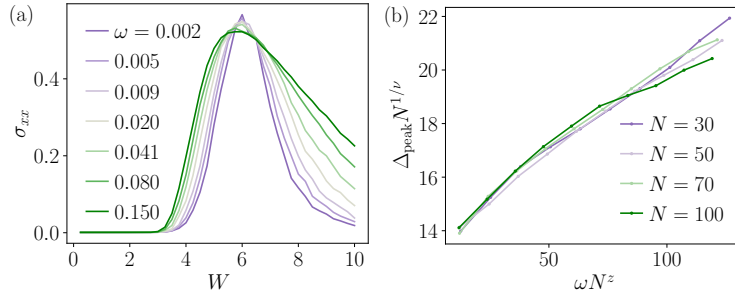


FIG. 4. (a) AC conductivity σ_{xx} as a function of disorder strength at various ω . (b) Full width at half maximum of σ_{xx} as function of the rescaled frequency ωN^z for different system sizes.

of these regions is increased as the disorder strength approaches the critical point. We estimate the typical length scale of these regions from the autocovariance function of the LCM,

$$R(r) = \frac{\sum_{|\mathbf{r}|=r} \sum_{\mathbf{r}'} c(\mathbf{r}') c(\mathbf{r}' + \mathbf{r})}{\sum_{|\mathbf{r}|=r} \sum_{\mathbf{r}'} c(\mathbf{r}')^2}. \quad (6)$$

We identify the typical length scale ξ in the LCM as the distance at which the autocovariance function crosses zero, $R(\xi) = 0$. The resulting disorder-averaged length scale as a function of rescaled disorder strength is shown in Fig. 2(c). By imposing the finite-size scaling ansatz and finding the best fit between curves for different system sizes, we find that $\nu = 2.5 \pm 0.3$. This matches the exponent obtained from the conductance and the Chern number and confirms that the LCM exhibits the critical length scale at the topological Anderson phase transition.

B. Dynamical critical exponent

Dynamical scaling of the IQHE has been measured from the critical behaviour of the conductance at a finite temperature or frequency of the driving electrical field [43–45]. A key feature, shared by both the IQHE and the disordered system considered here, is that the direct-current (DC) longitudinal conductivity vanishes away from the critical point, resulting in a singular peak at $W = W_c$ in the thermodynamic limit. At finite frequency, this singularity is broadened, giving rise to a peak in σ_{xx} with a finite width. Fig. 4(a) shows the conductivity as a function of disorder strength for different frequencies. The data clearly show the broadening of the conductivity peak as the frequency is increased. The finite width for frequencies tending to 0 is a consequence of the finite system size.

To characterize dynamical scaling, we analyze the scaling of the frequency-induced peak width. For a finite system, the conductivity depends on the ratio of the correlation length to the system size, ξ/N , and on the frequency through the dimensionless combination $\omega\tau_r$. Using the dynamical scaling relation $\tau_r \propto \xi^z$, the conductivity can be expressed with the scaling [46, 47]

$$\sigma_{xx}(\omega, W) = G_0 F(|W - W_c| N^{1/\nu}, \omega N^z). \quad (7)$$

Here, ωN^z defines the dimensionless time scale associated with the critical spreading over the system of size N . From Eq. (7), the scaling of the peak width follows directly as

$$\Delta_{\text{peak}}(\omega, N) = N^{-1/\nu} F(\omega N^z). \quad (8)$$

The finite-size scaling of the peak width is shown in Fig. 4(b). By optimizing the collapse of the rescaled curves as a function of z for a fixed $\nu = 2.5$ on the interval $\omega \in [\eta, 9\eta)$, we obtain $z = 1.96 \pm 0.07$. This is close to $z = 2$, which is the value found for other Anderson-type phase transitions for non-interacting fermions in two dimensions, including the IQHE [45]. This places the disordered Chern

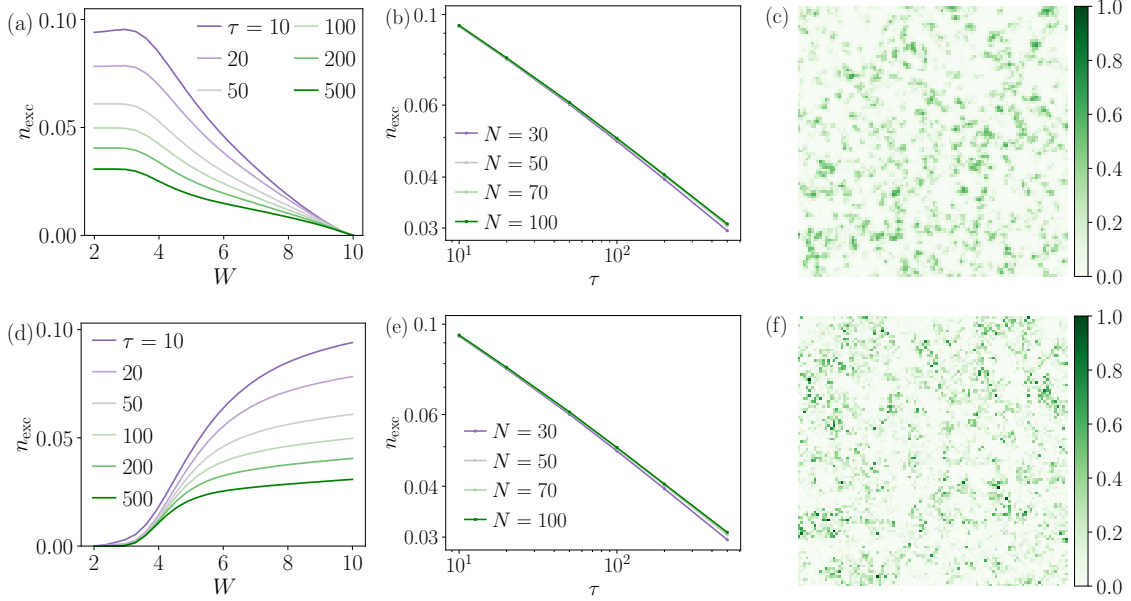


FIG. 5. Excitation density (a), (d) during quenches with different τ and (b), (e) at the end of the quench as a function of τ . (c), (f) show spatial distribution of excitations after a quench with $\tau = 10$ and $N = 100$. (a), (b) and (c) correspond to the trivial-to-topological protocol and (d), (e) and (f) to the topological-to-trivial protocol.

insulators in the same universality class as the IQHE for non-interacting fermions.¹

V. QUENCHES

In the following, we study systems driven linearly in time across the phase transition and analyze the resulting non-equilibrium dynamics in relation to ground-state critical properties. We consider quenches starting from the ground state at $u = -1$, where the disorder strength is varied linearly over a time τ from an initial value W_0 to a final value W_1 , $W(t) = W_0 + (W_1 - W_0)t/\tau$. Disorder landscape remains unchanged. We consider quenches in both directions: from the topological phase ($W_0 = 2$) to the trivial phase ($W_1 = 10$), and vice versa. During the quench, the spectral gap is closed due to localization, which drives the system out of equilibrium.

To describe the resulting non-equilibrium state, we calculate the density of excitations, defined as

$$n_{\text{exc}}(\mathbf{r}, t) = \sum_{\alpha} \langle \mathbf{r}\alpha | \hat{P}(t) \hat{P}_c(t) | \mathbf{r}\alpha \rangle. \quad (9)$$

Here, $\hat{P}(t) = \sum_n |\Psi_n(t)\rangle \langle \Psi_n(t)|$ is the projector onto the non-equilibrium occupied states and $\hat{P}_c(t)$ is the projector onto the unoccupied eigenstates of $H(t)$. Fig. 5(a) and Fig. 5(d) show the generation of excitations during quenches with different durations for both quench protocols. Due to the absence of the spectral gap for $W \gtrsim 2.5$, the time evolution is non-adiabatic, and excitations are generated continuously during the quench. The excitation generation rate is approximately constant and depends on the quench duration τ , leading to a τ -dependent excitation density at the end of the quench. This is shown in Fig. 5(b) and Fig. 5(e) for different system sizes. The final excitation density follows a power-law scaling with τ , with an exponent 0.281 ± 0.004 at $N = 100$ for both directions of the quench. The real space distribution of excitations is shown in Fig. 5(c) and Fig. 5(f) for both considered protocols.

¹ Experiments on IQHE found $z \approx 1$ [48], which is a consequence of electron interactions.

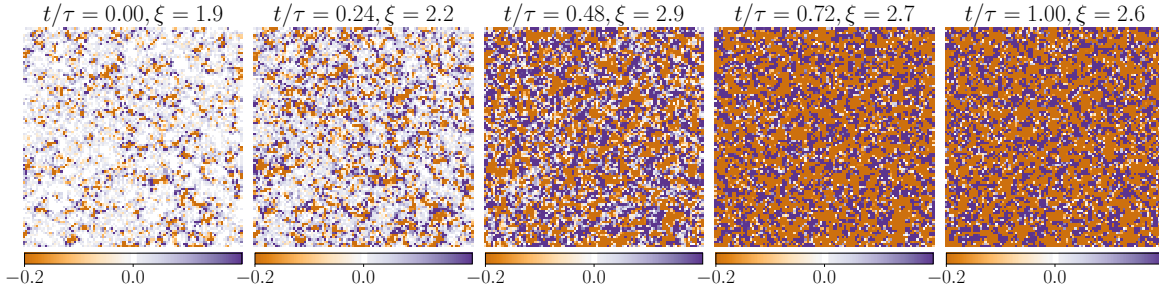


FIG. 6. Time evolution of the local Chern marker shown at different time slices during the trivial-to-topological quench with $\tau = 100$.

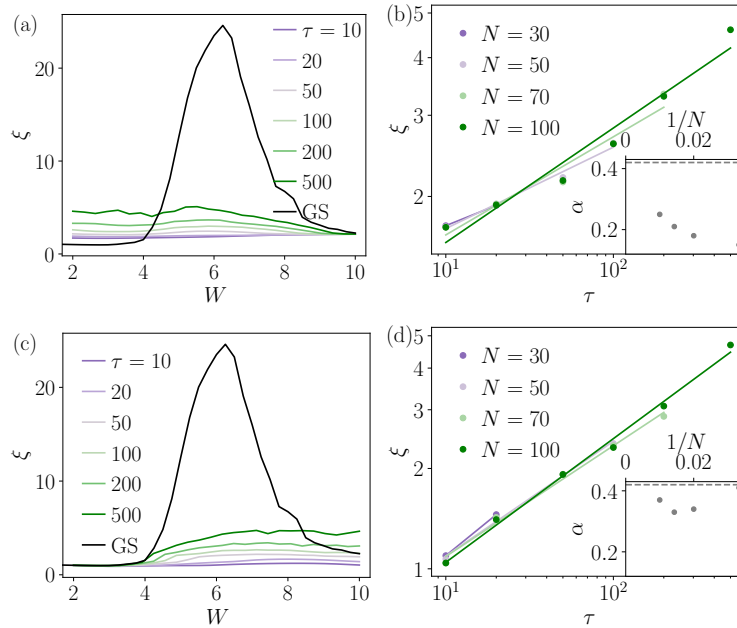


FIG. 7. Non-equilibrium length scale extracted from the profile of the LCM (a) during the trivial-to-topological quench and (c) during the topological-to-trivial quench for different quench durations. The black curve denotes the length scale in the ground state. The scaling of the final length scale with τ (b) for the trivial-to-topological quench and (d) for the topological-to-trivial quench.

The excitations are point-like due to the localization of eigenstates. In clean topological systems, it was shown that the excitation density follows the KZ scaling for defects with the power exponent $d\nu/(1+z\nu) = 0.85 \pm 0.03$ [25, 26, 32, 33], where the dimension $d = 2$. Our results clearly show that the excitation generation is not described by the KZ mechanism.

The LCM can be calculated for the non-equilibrium state by inserting the projector $\hat{P}(t)$ in Eq. (2). Fig. 6 shows the real-space profile of the LCM at different times during a quench with $\tau = 100$ from the trivial to the topological phase. As expected from Refs. [15, 25], the spatial average of the LCM, the Chern number, remains invariant throughout the evolution².

The non-equilibrium length scale in comparison to the ground-state correlation length is presented in Fig. 7(a) and Fig. 7(c). For the trivial-to-topological quench, it deviates from the adiabatic behaviour already at early times, while in the opposite direction, it follows the adiabatic curve until $W \approx 4$. The

² For long τ , the Chern number may change due to finite size effects.

dependence of this length scale on the quench duration is shown in Fig. 7(b) and Fig. 7(d)³. At the end of the quench, it exhibits a power-law scaling τ^α . For the topological-to-trivial quench we obtain $\alpha = 0.37 \pm 0.03$ for $N = 100$, which is close to the KZ prediction $\alpha = \nu/(1 + z\nu) = 0.42 \pm 0.01$. The values for smaller systems fluctuate (see inset to Fig. 7(d)), however they are all quite close to the KZ prediction. For the reverse direction, we get $\alpha = 0.20 \pm 0.04$ for $N = 100$, which deviates much more from the KZ prediction. The analysis of smaller system sizes indicates growth of α with increasing system size (see inset to Fig. 7(b)).

There are several aspects in which our results deviate from the standard KZ picture. When the quench is from the topological to the trivial side, we do see signatures of the freeze-out behaviour with characteristic growth of the LCM length scale with expected exponent. However, the freeze-out is not connected to the adiabaticity. For the quench with $\tau = 500$, the excitations in Fig. 5(d) appear already at $W \approx 2.5$ where the spectral gap closes, whereas the LCM length scale in Fig. 7(c) follows the ground state one until a much larger $W \approx 4.2$. This can be explained by LCM length scale being related to the mobility gap while the excitation generation to the closing of the spectral gap (see Fig. 1(c)). When the quench is from the trivial to the topological side, conversely, for studied system sizes both excitations and deviation of the LCM length scale from the groundstate value appear already at the beginning of the quench irrespectively how slow it is performed. On that side there is neither the spectral gap nor the mobility gap and it is difficult to imagine how KZ mechanism could operate. On the other hand, the LCM length scale does grow with the duration of the quench. The extracted critical exponent is not converged with respect to the system sizes and we cannot make a conclusive statement about the thermodynamic limit.

VI. CONCLUSION

We investigated the ground-state critical properties and the quench dynamics of strongly disordered Chern insulators. The disorder-driven phase transition occurs when the mobility gap closes, driving the system into a trivial Anderson insulating phase. This transition is signaled by a non-zero electrical conductivity and a change in the Chern number. The associated critical length scale manifests directly as the characteristic size of inhomogeneities in the real-space profile of the LCM. We extracted the critical exponents of the topological Anderson transition, $z = 2$ and $\nu \approx 2.5$, which fits the same universality class as the non-interacting IQHE. In contrast, experiments on the IQHE typically report a dynamical exponent $z = 1$, which is a consequence of electron–electron interactions. It would therefore be interesting to investigate whether a similar renormalization of z arises in disordered Chern insulators in the presence of interactions.

We further studied the non-equilibrium dynamics induced by quenches of the disorder strength across the phase transition. We found that the time evolution remains strongly non-adiabatic throughout the entire quench due to the absence of a spectral gap. Consequently, unlike in clean topological systems, the dynamics does not exhibit conventional Kibble–Zurek behaviour. In particular, the excitation density depends only weakly on the quench duration, indicating that the excitation dynamics is not governed by the equilibrium critical scaling. The quench-induced LCM length scale behaves differently depending on the direction of the quench. Within the observed system sizes, the LCM length scale is not captured by the KZ prediction for the trivial-to-topological quench. In the reverse direction, the LCM length scale is close to the KZ predictions. Its dynamics is decoupled from the excitation generation and may be influenced by the mobility gap instead.

An interesting direction for future work would be to extend this analysis to disordered topological systems in other symmetry classes, where different critical behaviour may emerge. In particular, disordered topological superconductors provide a promising platform, as they can host an metallic phase (the so-called Majorana metal) [6, 49, 50].

³ We omit the data where due to finite size effects the Chern number changes for more than 0.1.

ACKNOWLEDGMENTS

We thank L. Vidmar and J. C. Budich for interesting discussions and H. Torbatiyan for helpful comments.

Funding information This work was supported by the Slovenian Research and Innovation Agency (ARIS) under contracts no. P1-0044 and J1-50005. G. Lemut acknowledges support by the Deutsche Forschungsgemeinschaft (DFG, German Research Foundation) as part of the German Excellence Strategy - EXC3112/1 - 533767171 (Center for Chiral Electronics).

* lara.ulcakar@fmf.uni-lj.si

- [1] M. Z. Hasan and C. L. Kane, *Rev. Mod. Phys.* **82**, 3045 (2010).
- [2] C.-Z. Chang, J. Zhang, X. Feng, J. Shen, Z. Zhang, M. Guo, K. Li, Y. Ou, P. Wei, L.-L. Wang, Z.-Q. Ji, Y. Feng, S. Ji, X. Chen, J. Jia, X. Dai, Z. Fang, S.-C. Zhang, K. He, Y. Wang, L. Lu, X.-C. Ma, and Q.-K. Xue, *Science* **340**, 167 (2013).
- [3] M. M. Otrokov, I. I. Klimovskikh, H. Bentmann, D. Estyunin, A. Zeugner, Z. S. Aliev, S. Gaß, A. U. B. Wolter, A. V. Koroleva, A. M. Shikin, M. Blanco-Rey, M. Hoffmann, I. P. Rusinov, A. Y. Vyazovskaya, S. V. Ereemeev, Y. M. Koroteev, V. M. Kuznetsov, F. Freyse, J. Sánchez-Barriga, I. R. Amiraslanov, M. B. Babanly, N. T. Mamedov, N. A. Abdullayev, V. N. Zverev, A. Alfonsov, V. Kataev, B. Büchner, E. F. Schwier, S. Kumar, A. Kimura, L. Petaccia, G. Di Santo, R. C. Vidal, S. Schatz, K. Kißner, M. Ünzelmann, C. H. Min, S. Moser, T. R. F. Peixoto, F. Reinert, A. Ernst, P. M. Echenique, A. Isaeva, and E. V. Chulkov, *Nature* **576**, 416–422 (2019).
- [4] M. Serlin, C. L. Tschirhart, H. Polshyn, Y. Zhang, J. Zhu, K. Watanabe, T. Taniguchi, L. Balents, and A. F. Young, *Science* **367**, 900–903 (2020).
- [5] E. Prodan, T. L. Hughes, and B. A. Bernevig, *Phys. Rev. Lett.* **105**, 115501 (2010).
- [6] M. V. Medvedyeva, J. Tworzydło, and C. W. J. Beenakker, *Phys. Rev. B* **81**, 214203 (2010).
- [7] J. Mildner, M. D. Caio, G. Möller, N. R. Cooper, and M. J. Bhaseen, *Topological phase transitions in the disordered haldane model* (2023), arXiv:2312.16689 [cond-mat.str-el].
- [8] D. J. Salib and B. Roy, *Phys. Rev. B* **112**, L180201 (2025).
- [9] J. T. Chalker and P. D. Coddington, *Journal of Physics C: Solid State Physics* **21**, 2665–2679 (1988).
- [10] B. Huckestein and B. Kramer, *Phys. Rev. Lett.* **64**, 1437 (1990).
- [11] A. W. W. Ludwig, M. P. A. Fisher, R. Shankar, and G. Grinstein, *Phys. Rev. B* **50**, 7526 (1994).
- [12] J. Priest, S. P. Lim, and D. N. Sheng, *Phys. Rev. B* **89**, 165422 (2014).
- [13] M. Moreno-Gonzalez, J. Dieplinger, and A. Altland, *Annals of Physics* **456**, 169258 (2023).
- [14] S. Bera, J. Dieplinger, and N. P. Nayak, *Phys. Rev. B* **109**, 174213 (2024).
- [15] M. D. Caio, N. R. Cooper, and M. J. Bhaseen, *Phys. Rev. Lett.* **115**, 236403 (2015).
- [16] H. Dehghani and A. Mitra, *Phys. Rev. B* **93**, 205437 (2016).
- [17] M. D. Caio, N. R. Cooper, and M. J. Bhaseen, *Phys. Rev. B* **94**, 155104 (2016).
- [18] F. N. Ünal, E. J. Mueller, and M. O. Oktel, *Phys. Rev. A* **94**, 053604 (2016).
- [19] Y. Hu, P. Zoller, and J. C. Budich, *Phys. Rev. Lett.* **117**, 126803 (2016).
- [20] L. Privitera and G. E. Santoro, *Phys. Rev. B* **93**, 241406(R) (2016).
- [21] J. H. Wilson, J. C. W. Song, and G. Refael, *Phys. Rev. Lett.* **117**, 235302 (2016).
- [22] P. Wang, M. Schmitt, and S. Kehrein, *Phys. Rev. B* **93**, 085134 (2016).
- [23] U. Bhattacharya, J. Hutchinson, and A. Dutta, *Phys. Rev. B* **95**, 144304 (2017).
- [24] M. Schüler and P. Werner, *Phys. Rev. B* **96**, 155122 (2017).
- [25] L. Ulčakar, J. Mravlje, A. Ramšak, and T. Rejec, *Phys. Rev. B* **97**, 195127 (2018).
- [26] L. Ulčakar, J. Mravlje, and T. Rejec, *Phys. Rev. B* **100**, 125110 (2019).
- [27] M. McGinley and N. R. Cooper, *Phys. Rev. B* **99**, 075148 (2019).
- [28] M. McGinley and N. R. Cooper, *Phys. Rev. Lett.* **121**, 090401 (2018).
- [29] S.-F. Liou and K. Yang, *Phys. Rev. B* **97**, 235144 (2018).
- [30] T. W. B. Kibble, *Journal of Physics A: Mathematical and General* **9**, 1387 (1976).
- [31] W. H. Zurek, *Nature* **317**, 505 (1985).
- [32] B. Damski, *Phys. Rev. Lett.* **95**, 035701 (2005).
- [33] A. Dutta, R. R. P. Singh, and U. Divakaran, *EPL (Europhysics Letters)* **89**, 67001 (2010).
- [34] L. Ulčakar, J. Mravlje, and T. Rejec, *Phys. Rev. Lett.* **125**, 216601 (2020).
- [35] Z. Sun, M. Deng, and F. Li, *Phys. Rev. B* **106**, 134203 (2022).
- [36] H. Yuan, J. Zhang, S. Chen, and X. Nie, *Phys. Rev. B* **110**, 165130 (2024).

- [37] B. Altshuler, H. Krovi, and J. Roland, *Proceedings of the National Academy of Sciences* **107**, 12446–12450 (2010).
- [38] X.-L. Qi, Y.-S. Wu, and S.-C. Zhang, *Phys. Rev. B* **74**, 085308 (2006).
- [39] R. Favata, N. Baù, and A. Marrazzo, *Phys. Rev. Lett.* **135**, 026603 (2025).
- [40] R. Bianco and R. Resta, *Phys. Rev. B* **84**, 241106(R) (2011).
- [41] C. W. Groth, M. Wimmer, A. R. Akhmerov, and X. Waintal, *New Journal of Physics* **16**, 063065 (2014).
- [42] M. L. Mehta, in *Random Matrices*, Pure and Applied Mathematics (Amsterdam) (Elsevier, 2004) pp. xiii–xiv.
- [43] H. P. Wei, D. C. Tsui, M. A. Paalanen, and A. M. M. Pruisken, *Phys. Rev. Lett.* **61**, 1294 (1988).
- [44] L. W. Engel, D. Shahar, i. m. c. Kurdak, and D. C. Tsui, *Phys. Rev. Lett.* **71**, 2638 (1993).
- [45] B. Huckestein, *Rev. Mod. Phys.* **67**, 357 (1995).
- [46] Y. Avishai and J. M. Luck, *Dynamical critical behavior in the integer quantum hall effect* (1996).
- [47] L. Schweitzer, Frequency dependent electrical transport in the integer quantum Hall effect, in *Anderson Localization and Its Ramifications* (Springer Berlin Heidelberg, 2003) p. 65–82.
- [48] F. Evers and A. D. Mirlin, *Rev. Mod. Phys.* **80**, 1355 (2008).
- [49] J. T. Chalker, N. Read, V. Kagalovsky, B. Horowitz, Y. Avishai, and A. W. W. Ludwig, *Phys. Rev. B* **65**, 012506 (2001).
- [50] V. A. Zakharov, I. C. Fulga, G. Lemut, J. Tworzydło, and C. W. J. Beenakker, *New Journal of Physics* **27**, 033002 (2025).